FORSCHUNGSZENTRUM
ROSSENDORF e.V.

FZR

FZR 93 - 21
October 1993

G. Hessel, W. Schmitt and F.-P. Weiß

Acoustic Leak Detection at Complicated Geometrical Structures Using Fuzzy Logic and Neural Networks

Acoustic Leak Detection at Complicated Geometrical Structures Using Fuzzy Logic and Neural Networks

G. Hessel, W. Schmitt, and F.-P. Weiß
Research Center Rossendorf, Inc.

CONTENTS

ABSTRACT

Methods of acoustic leak monitoring are of great practical interest for the safety of pressure vessels and pipe lines not only at the primary circuit of nuclear power plants. In this report some aspects of acoustic leak localization at complicated three-dimensional topologies for the case of leakage monitoring at the reactor vessel head of a VVER-440 are discussed.

Existing acoustic methods, using the attenuation or the propagation time differences of the airborne sound or structure-borne sound, are inadequate at such complicated structures especially when the thickness of the pressure confining walls is not great enough to allow the full development of a surface wave.

Therefore, an acoustic method based on pattern recognition is being developed. During the learning phase, the localization classifier is trained with sound patterns that are generated with simulated leaks at all locations endangered by leak. The patterns are extracted from the signals of an appropriate sensor array. After training unknown leak positions can be recognized through comparison with the training patterns.

The experimental part of the task is performed at an acoustic 1:3 model of the reactor vessel head and at an original VVER-440 reactor in the former NPP Greifswald. At the Greifswald VVER-440 the leaks were simulated at the vessel head using mobile sound sources driven either by compressed air, a piezoelectric transmitter or by a thin metal blade excited through a jet of compressed air.

The sound patterns of the simulated leaks are simultaneously detected with an AE-sensor array and with high frequency microphones measuring structure-borne sound and airborne sound, respectively.

Pattern classifiers based on Fuzzy Pattern Classification (FPC) and Artificial Neural Networks (ANN) are currently tested for

- the validation of the AE-sensor array (FPC)
- the leak localization via structure-borne sound (FPC) and
- the leak localization using microphones (ANN).

The initial results show the used classifiers principally to be capable of detecting and locating leaks, but they also show that further investigations are necessary to develop a reliable method applicable at NPPs.

1. Introduction

Methods of acoustic leak monitoring are of great practical interest for the safety of pressure vessels and pipe lines not only at the primary circuit of nuclear power plants. A sophisticated leakage monitoring system must be capable of detecting a leak promptly, locating it and eventually, if possible, estimating the leak rate.

In recent years, acoustic leak monitoring systems have been developed to detect and localize leaks at simple geometrical structures such as pipe lines and pressure vessels, which have a smooth surface and only a small number of connection branches and connection lines, respectively.

Existing acoustic methods, using the attenuation [1] or the propagation time differences [2] of the airborne sound or structure-borne sound, are inadequate at complicated structures especially when the thickness of the pressure confining walls is not great enough to allow the full development of a surface wave.

To enhance also the safety of pressure confining vessels with complicated structure, a new method based on pattern recognition is being developed for detecting and localizing leaks at such topologies. In the following, various pattern classification systems used for leak localization and results obtained through leak simulation experiments at an original pressure vessel head of a VVER-440 in the Nuclear Power Station Greifswald are represented.

2. Aspects of Leak Monitoring at the Pressure Vessel Head of VVER-440 Reactors

This task results from many leaks that occurred at VVERs operated in Central and Eastern Europe. The problem was also addressed in VVER safety reports, released by the IAEA and by the GRS Cologne [3, 4]. Accordingly, it was recommended to develop and to install leak detecting and localizing systems at this VVER component.

The scheme in Fig. 1 can only indicate the structure of the reactor vessel head and schematically show what could happen in the case of an unidentified leak. The vessel head construction consists of the upper calotte, 37 standpipes containing the control element drives, and 18 connecting branches for incore sensors at the periphery. Totally there are about 100 flanges in different heights and 37 circumferential weldings between the ferrite pressure vessel steel and the austenite of the standpipe. All these elements are especially endangered by leaks.

Leaks in this region of the primary circuit do not only result in a loss of coolant but might also lead to a standpipe tear off followed by the control element ejection.

Conventional leak monitoring methods, such as measuring the released radioactivity and/or moisture, fail because there is an air circulation of 80 000 m^3 /h under the protective cover (Fig. 1). Even the well known leak localization methods, based on the attenuation [1] or propagation time differences [2] of the structure-borne sound, are not applicable due to

the complexity of the structure and because surface or Rayleigh waves cannot fully develop because the thickness of the standpipe walls is not great enough.

Fig. 2 showing the cross-correlation function between two Acoustic Emission (AE)-sensor signals measured at the pressure vessel head (see also Fig. 8) demonstrates the calamity of propagation time investigations. Multiple propagation paths with and without reflection and the different sound modes generate a great number of maxima in the cross-correlation function. There is no clear maximum that could be used for the leak localization.
A similar confusing constellation is found when the attenuation method is used, because it can only successfully be applied if one sound mode is clearly predominating.

Nevertheless there is a strong need to provide a method permitting sensitive and reliable leak localization at the vessel head and at pressurized systems confining dangerous fluids in general.

3. Working Principle

It is the idea of the new method, illustrated in Fig. 3, to use sophisticated pattern classification systems for leak localization at three-dimensional topologies. In the learning phase, the pattern classifier is trained using a mobile source of sound simulating the leak at all positions, endangered by leaks. The sound is measured by a multisensor array mounted at the structure. RMS-values, components of power spectra or coherence functions are used to extract the feature vector for each leak location.
After having trained the classifier for all positions, in the recall or classification phase,unknown leaks can be localized.
Various types of classifiers were used for these purposes, for example

- Fuzzy Pattern Classification System MICRO FUCS /5/
- Artificial Neural Network Classification System NEUROPRO /6/.

4. Leak Simulation Experiments at a VVER-440

To prepare the experiments at the VVER reactor, an acoustic model of the reactor pressure vessel head was built. Fig. 4 shows the scheme of the acoustic model. The geometrical dimensions of the reactor pressure vessel head (upper block) were transferred (scale 1:3) to a thick plate made from cast iron.
To investigate the influence of sound reflections at flanges and holes, the acoustic model was completed in different steps. A step with 60% of the holes of the standpipe is shown in Fig. 4.

The acoustic model was also used to test various sound sources for leak simulation.
Depending on the specific aim different mobile sound sources were used, so for example

- a source using a jet of compressed air
- an acoustic emission sensor in the transmitting mode and

- a thin metal-blade, coupled to the structure with silicon oil and excited through a jet of compressed air (see Fig. 5).

Fig. 6 shows the measuring and signal processing equipment for the leak simulation experiments at an original reactor pressure vessel head in the former Greifswald Nuclear Power Station.
Twelve AE-sensors directly mounted at the structure and three high frequency microphones installed at the wall of the protection vessel that forms a sound boundary around the reactor pressure vessel head were used. The microphones served both for intensity monitoring of simulated leaks and leak localization.

All the AE-sensors could also be operated in the transmitting mode what is necessary for the calibration of the AE-sensor array and for the simulation of leak noise as well.
The high frequency sound signals from the AE-sensors were simultaneously measured up to 500 kHz.The microphone signals were acquired up to 70 kHz. The signals could either be stored on the analog magnetic tape recorder or digitally on disks and cartridges.
Up to now learning and classification have been performed off-line.

The positions of AE-sensors, microphones and simulated leak positions are depicted in Fig. 7. Here a sound source based on a compressed air jet was used, while Fig. 8 gives the leak positions when sound was emitted from the metal-blade excited to high frequency vibrations by a compressed air jet. In both figures the air jet direction is indicated by arrows. Leak L5 in Fig.7 was located on the top of a standpipe being 7 m long. The other leaks in Fig.7 and Fig.8 were at the flange of the standpipe and at the connecting branch for incore sensors.

In the following, first results obtained by using different signals and different classifiers are discussed.

5. Leak Localization by a Fuzzy Pattern Classifier

5.1 Fuzzy Pattern Classification

The fuzzy concept is utilized for leak localization to consider the existing uncertainties in the interpretation of the classes and in the recognition of a class. These uncertainties come from fluctuations of the leak sound intensity, from variations of the leak sound spectrum over the time, from different spectra for different leaks, respectively, and from disturbances during the measurement. Fuzzy sets are defined as sets of which the boundaries are not clearly defined. The fuzzy subset A_k of the feature space R is described by its membership function μ_k. The membership functions μ_k ($k = 1,2 \ldots K$) map the elements $\underline{X}$ of the feature space to the continuous interval [0,1]

$$\mu_k\ (\underline{X}) \rightarrow [0,1] \quad \text{for all } k = 1,2,\ldots,K. \tag{1}$$

If A_k represents a certain class of events, $\mu_k(\underline{X})$ expresses the degree of membership of $\underline{X}$ to the class k. This is in contrast to "crisp sets" with sharp boundaries where the membership

function is either

$$\mu_k (\underline{X}) = 1 \text{ or } \mu_k (\underline{X}) = 0, \tag{2}$$

depending on $\underline{X}$ is an element of the class k or not.

The concept of the membership function can be used to quantify the degree of belongingness of a pattern $\underline{X}$ to all classes $k = 1,2, \ldots, K$ assumed to be fuzzy sets.

For fuzzy pattern classification the PC-code MICRO FUCS developed at the Technical University of Chemnitz-Zwickau is used [5]. This classification model is based on fuzzy sets in a high-dimensional feature space.

As features, pure measuring data, characteristic values obtained from special signal pre-processing or certain values of statistical characteristic functions can be used. So a pattern is a feature vector $\underline{X}$ with the features X_i being its elements. $\underline{X}$ is represented by a point in the multidimensional space

$$\underline{X} = [X_1, X_2, \ldots, X_I]^T. \tag{3}$$

The K classes are assigned to the subsets A_k $(k = 1, 2, .., K)$ during a so called training phase.
The task of the classification of an unknown pattern is to find the area to which the unknown feature vector belongs. The difference between the fuzzy pattern recognition and the classical ones lies in the fact that the separate classes are defined to be fuzzy themselves, so that each pattern is not associated with only one class but with all the possible classes by means of a membership vector

$$\underline{\mu}(\underline{X}) = [\mu_1(\underline{X}), \mu_2(\underline{X}), \ldots, \mu_K(\underline{X})]^T \tag{4}$$

in the fuzzy decision space $[0, 1]^K$.
MICRO FUCS uses potential functions as parametric membership function. For only one feature the membership function is given by

$$\mu_k (x_i) = \frac{1}{1 + \left| \frac{X_i - X_{ik}}{C_{ik\pm}} \right|^{d_{ik\pm}}} \tag{5}$$

where the parameters mean

X_{ik} component i of the domain center k
$c_{ik\pm}$ "distance" of the left (-) and right (+) margin from the center X_{ik} in direction i

$d_{ik\pm}$ exponent defining the slope of the drop on the left (-) and right (+) side of the potential function in direction i

These parameters are adapted in the training phase by using either measuring data or characteristic statistical values or a priori knowledge or even a combination of that. If X_i is left of X_{ik}, c_{ik-} and d_{ik-} have to be used, while c_{ik+} and d_{ik+} must be taken if X_i is right of X_{ik}. Membership functions are shown in Fig. 10 for the two features M8 and M9. Here the membership functions are denoted by L1, L2, ..., L8. When these five parameters are known for all classes and for all features, the degrees of the membership of a feature vector $\underline{X}$, sometimes called sympathy, can be determined for all classes.
The sympathy of the vector $\underline{X}$ with respect to class number k is obtained by summing up over all features X_i in the way suggested by equation (6)

$$\mu_k(\underline{X}) = \frac{1}{1 + \sum_i \left| \frac{X_i - X_{ik}}{c_{ik\pm}} \right|^{d_{ik\pm}}} \qquad (6)$$

Also $\mu_k(\underline{X})$ assumes values between 0 and 1. The final result of a fuzzy classification is then given by the sympathy vector $\underline{\mu}(\underline{X})$ of equation (4). All $\mu_K(\underline{X})$ are its elements.

To reduce the risk of misclassification, the following rules are implemented in MICRO FUCS

1. A feature vector is only unambiguously assigned to class j by the maximum sympathy $\mu_j(\underline{X})$ if this value is considerably larger than all the other ones and fulfills the equation

$$\mu_j(\underline{X}) \cdot S \geq \mu_k(\underline{X}) \quad \text{for all } k \neq j \qquad (7)$$

where $\mu_j(\underline{X})$ is given by

$$\mu_j(\underline{X}) = \max_k [\mu_k(\underline{X})] \qquad (8)$$

S is a threshold factor preset by the user and determines the maximum sympathy ratio

$$S = \frac{\max_{k \neq j} [\mu_k(\underline{X})]}{\mu_j(\underline{X})} \qquad (9)$$

that is still allowed for unambiguous assignment. A small value of S means that a great distance is demanded between the greatest and the second greatest sympathy.

2. A feature vector is assigned to class j with risk if

$$\mu_j(\underline{X}) \cdot S \geq \mu_k(\underline{X}) \text{ for all } k \neq j, 1 \qquad (10)$$

where the second greatest sympathy $\mu_1(\underline{X})$ follows from

$$\mu_1(\underline{X}) = \max_{k \neq j} [\mu_k(\underline{X})] \qquad (11)$$

Consequently, for risk assignment

$$\mu_k(\underline{X}) \cdot S < \mu_1(\underline{X}) \qquad (12)$$

is valid.

3. A pattern is rejected by the fuzzy classifier if its sympathies to all classes $\mu_k(\underline{X})$ are less than a threshold μ_{min}

$$\mu_k(\underline{X}) < \mu_{min} \text{ for all } k = 1, 2, \ldots, K. \qquad (13)$$

The results discussed in the following are based on the sympathy threshold $\mu_{min} = 0.1$ and on the threshold factor $S = 0{,}3$.

5.2. Results obtained by fuzzy classifier MICRO FUCS

The capability of the fuzzy pattern classifier to recognize and to localize leaks by means of RMS-values of structure-borne sound was tested.
The RMS-values of the sensors AE 1 to AE 12 were measured for eight different simulated leak positions L 1 to L 8 (Fig.8). Two leak positions at the same standpipe mean that the simulating sound was introduced into the structure at "opposite" positions of the same flange. To eliminate the disturbing influences of leak intensity fluctuations, all RMS-values were normalized with the sum of all 12 values.

Initially, a classifier A was trained to differ between all the eight positions, that means even between those at the same standpipe as for instance leaks L4 and L5 (see Fig. 8).
The result is shown in the upper part of Fig. 9 for two features M 8 and M 9. And as it should be expected there is really a small distance between leak positions L4 and L5 in the feature space.

Contrary looking at positions L7 and L8 also being simulated at the same standpipe it should be noticed that there is a greater difference between these two than between positions L1 and L2 being far apart from each other. This exhibits the difficulties that the known leak monitoring systems would have.
It is necessary to explain that the lines in the two-dimensional plots represent the isogram of the sympathy function over the two-dimensional feature space.
Generally, a satisfying separation of all classes can be stated. The classification using all 12 features confirms the separability of the simulated leak positions. The classifier rejects some feature vectors as not to be classifiable but it provides no wrong classification.

Since it is not really the aim of the method to be developed to distinguish between leaks at the same standpipe flange but with different direction of sound radiation, the classes L4, L5 on the one hand and L7, L8 on the other hand were united. This unification provides the new classes L4: L4/L5 and L6: L7/L8, respectively.

The classifier B was trained with this situation. Consequently, the new membership functions L 4/5 become wider than before but the separability of the new classes with respect to the others is conserved, as can be taken from the membership functions belonging to features M 8 and M 9 (Fig. 10) and as can also be seen from the sympathy-isoplots in the lower part of Fig. 9. Moreover, by using only six classes the number of rejections is decreased while no wrong classifications are obtained.

Summarizing, it can be said that it seems hopeful to achieve a complete separation of leaks at all flanges by means of measuring RMS-values of about 12 to 16 acoustic emission sensors and by applying a fuzzy classifier.
To decide finally about the capability of this method, further simulation experiments are necessary.

6. Leak Localization through Artificial Neural Networks

6.1 Artificial Neural Networks - Basic Remarks

In these investigation four different neural networks have been used:

- a two-layer perceptron (P1) network with error backpropagation,
- a three-layer perceptron (P2) network with error backpropagation,
- a condensed nearest neighbour (CCN) network and
- a counterpropagation (CPP) network.

The working principle of an artificial neural network is illustrated by means of the structure of a three-layer perceptron (P2) network with error backpropagation as it is shown in Fig. 11.

Multilayer Perceptron Network with Error Backpropagation

The P2 network consists of an input layer, a hidden layer and an output layer. The number of neurons in the input and output layer respectively is equivalent to the number of the features I in the feature vector and to the number of classes K. Obviously the number of classes K corresponds with the number of leak positions to be identified. To form the output value O_j, each neuron weights the outputs O_i of the neurons in the previous layer with its connection strengths W_{ji} and squashes the sum of the weighted inputs with a sigmoid or squashing function f(X).
This procedure is schematically shown in Fig. 11b for a neuron in the hidden layer.
The notation in Fig. 11 is based on the following convention where i is the index of the input layer, j is the index of the hidden layer and k is the index of the output layer.
To supervise the training phase of perceptron networks, the feedforward output state calculation is combined with backward error propagation leading to an adjustment of the weights (connection strengths) to minimize the summed error of the activity of the neurons in the output layer.

$$E = \frac{1}{2}\sum_{k} (L_k - O_k)^2 \rightarrow \min \qquad (14)$$

L_k is the desired, O_k the really obtained output state.
Minimizing equation (16) results in the well known recursive prescriptions for updating the connection strengths.
The new connection strengths W_{kj}^* between the output layer and the hidden layer follow from

$$W_{kj}^* = W_{kj} + \alpha\, \delta_k\, X_j \qquad (15)$$

where α is a learning rate chosen by the user in advance, X_j mean the outputs of the hidden layer, and δ_k is given by

$$\delta_k = f'(\sum_{j} W_{kj}X_j) \cdot (L_k - O_k) \qquad (16)$$

where $f'(\Sigma\, W_{kj}X_j)$ is the derivative of the sigmoid function in neuron k of the output layer.
In analogy for the new connection strengths W_{ji}^* between input and hidden layer one gets

$$W_{ji}^* = W_{ji} + \alpha\, \delta_j\, X_i \qquad (17)$$

with

$$\delta_j = f'(\sum_i W_{ji}X_i) \cdot \sum_j W_{kj}\,\delta_k \qquad (18)$$

where $f'(\Sigma\, W_{ji}X_i)$ is the derivative of the sigmoid function in neuron j of the hidden layer.

Formulas (15) to (18) are derived in detail in [7].

There are as well hidden layer networks with a fix and predetermined number of neurons in the hidden layers as also networks being able of learning the suited number of neurons. The number of hidden layer neurons of the three-layer perceptron (P2-network) is predetermined for instance, while it is learned during training for the condensed nearest neighbour (CNN) network.

Condensed Nearest Neighbour Network

To be able to understand the following, it must be mentioned that CNN networks, though having the same topology as the P2 perceptron, realize a rather different algorithm. Instead of the connection strengths, the hidden layer neurons are characterized by prototype vectors. In the simplest case there might be as many hidden layer neurons as training vectors. Then each neuron were characterized by its own training vector.

Further the hidden layer neurons of a CNN network dispose of a vector $\underline{r}$ describing the receptive field around the tip of the prototype vector. Fig. 15 shows two-dimensional receptive fields (features M171 and M93). The inputs of the hidden layer neuron j are a specially defined distance d_j between the prototype vector $\underline{W_j}$ and the feature vector $\underline{X}$.
d_j follows from

$$d_j = \sqrt{(\sum_i d_{ji}^2)} \qquad (19)$$

where the distance d_{ji} in direction i of the feature space is determined through

$$d_{ji} = \max\,(0,\ |W_{ji} - X_i| - r_i) \qquad (20)$$

So if $\underline{X}$ is in the receptive field of the neuron, d_{ji} will be set zero, otherwise it is the real distance reduced by r_i. The output of the hidden layer neuron is given by

$$O_j = 2e^{-d_j/2} - 1 \qquad (21)$$

One more peculiarity of CNN networks is the fact that the connection strengths V_{kj} between the output neuron k and the hidden layer neuron j can only assume the values 0 or 1. The output O_k is the maximum of the offered weighted inputs X_j from hidden layer neurons j

$$O_k = \max_j \; [V_{kj} X_j] \qquad (22)$$

6.2 Results

The capability of the different neural network types to recognize leak locations by means of the high frequency microphone signals was tested.
Fig. 7 shows the positions MICn of the microphones and the positions of the simulated leaks Lm. Leaks were simulated with a jet of compressed air. The arrows in Fig. 7 indicate the jet direction. L5 was simulated at the top of a standpipe.

It was found that the coherence functions between the two high frequency microphones provide suitable feature vectors characterizing the source location of the airborne sound. Certainly the reason for this is that each leak position results in a typical fictive nonlinear sound propagation from the one to the other microphone. And this special nonlinear transfer determines the coherence function. Moreover, using the coherence, the spectral changes of the leak noise over the time do not influence the classification. Therefore, the 200 points of the coherence function were taken as features.

Fig. 12 compares two coherence functions connected with leak positions L1 and L6, respectively. Leak L1 provides high coherence at the feature number M171, which corresponds to a frequency of 43 KHz, while leak L6 gives high coherence at lower frequencies. It has to be explained that when looking closely to the Fig. 12, three curves can be resolved, a dark-blue representing a single pattern and two light-blue curves, showing the $\pm \sigma$ - dispersion range of those coherence functions used for training.

The dispersion range is needed to exclude strongly deviating patterns from learning, as they might result from disturbing noise at a running nuclear power plant.

To compare the suitability of the different mentioned network types, the same training patterns were used for all networks.

The two-layer P1 perceptron is a quickly learning network, because it can be started with high learning rates, controlled by a positive constant α of about 0.5, and enables a fast adjustment of the connection strengths between the neurons by the error backpropagation procedure. As can be seen from the upper part of Fig. 13 the maximum classification error (light blue coloured) and the average classification error (dark blue) quickly decrease after only a few training cycles. But it is important to remark that the learning rate α must be decreased from cycle to cycle to avoid that the classification error increases again or begins to oscillate.

The colour spectrum in the lower part of Fig. 13 indicates the connection strengths (or weights) of the selected output neuron to the input neurons receiving the coherence function. Red and yellow lines mean high connection strengths and high weights for the classification (into class number 5 here), while blue and green lines indicate zero or low weight.

It must be considered that P1 networks can only successfully be applied when the classes can be linearly separated by the used features. And as the results show this seems to be the case in the application discussed. Otherwise a counterpropagation network with a two-dimensional hidden layer that is capabable of even differing between classes which are only non-linearly separable could be used to search for subclasses. Then using these subclasses it might become possible to apply the P1 network successfully.
The classes do not fall into subclasses when all hidden layer neurons connected with a selected output neuron are located in a linked area of the two-dimensional hidden layer of the counterpropagation network.

An example with 64 neurons in the hidden layer is shown in Fig. 14 as square Kohonen-map. All neurons that were not exclusively connected to one and the same output neuron during the last training cycles were cancelled and are labelled with a question mark.

Since the areas pertaining to the several output neurons are linked for all classes this proves that there are no subclasses.
So if the P1 network would fail the subdivision into subclasses would be no way out of the calamity.

For the purposes pursued it is a considerable disadvantage of the Kohonen counterpropagation network that complete training takes about one hour.
Excepting the counterpropagation network, a reclassification rate of 100% was achieved with all classifiers when assigning the patterns that have also been used for the training.

In spite of rather short training times (only a few minutes) the two layer P1 perceptron achieves excellent classification results. 19 patterns pertaining to class 2 but unknown to the network were classified without error. Fig. 16 shows a typical feature vector, the number of patterns to be classified and where they were assigned to. The table in the upper part of the figure gives the values of the 7 output neurons. Neuron two only gives values very near to 1, that is 98% to 99%, while the others provide zero for patterns 13 to 19.

The counterpropagation network Fig. 17 though not achieving a complete reclassification was also capable of correctly classifying all patterns. But it has to be noticed that the separability is considerably worse. All output neurons provide values not equal to zero.
Consequently, this network should not be used in applications requiring high classification accuracy and low rejection rates. For the same class 1 the minimum difference between output of neuron 1 and other neurons in the output layer is only 0.20.

Fig. 18 displays the situation for the condensed nearest neighbour (CNN) network. With respect to the counterpropagation network the separability is improved, the minimum absolute difference is 0.49, but it is still worse than for the two perceptron networks.

The CNN network rejected pattern number 19 as not to be classifiable to a certain class. That is correct, because pattern 19 was extracted from an incomplete time series of the sound signal that means only about 50% of the sweep was filled with correct samples and the rest was set to zero. The rejection of the resulting pattern hints at the efficiency of the method: instead of a misclassification a rejection is made.

Fig. 19 shows the results obtained with the three-layer perceptron P2. In contrast to the P1 network where patterns of class 2 were to be classified here 16 patterns from class 1 were offered. Again the excellent separability is obtained. All output neurons not belonging to class 1 really provide zero.

7. Conclusion

Finally it can be stated:

1. Both investigated perceptron networks are appropriate means for localizing leaks at the three-dimensional topology and the coherence is a suitable function of which significant features can be extracted from.

2. For very great numbers of classes, 100 or even more, as it is the case for the pressure vessel head, the P1 network seems best suited, since the high number of neurons in the hidden layer of the P2 network leads to very long times for the training. The training time is about two orders of magnitude longer for P2 than for P1.

3. Generally the application of high frequency microphones for the localization of leaks at a complex structure contained in a room with walls reflecting the airborne sound seems to be a promising approach. Nevertheless one must be aware of the fact, which was not yet discussed in connection with neural networks that the detected airborne sound signal does not only depend on the leak position but also strongly on the directional characteristic of the radiated sound. This needs further investigation.

4. Therefore, the measurement of the RMS-values of the acoustic emission sensor signals is needed as complementary approach. Though there is also a dependence on the sound radiation direction, the influence of the leak positions seems to predominate.

5. The most important future step will be the application of neural networks to the acoustic emission sensor signals, to coherence between them, to RMS-values, and to power spectra as well.

References

[1] Jax, P., K. Ruthrof
Acoustic Emission Inspections of Nuclear Components Considering Recent Research Programmes
Nuclear Engineering and Design 113 (1989) 71 - 79

[2] Fuchs, H. V., R. Riehle
Ten Years of Experience with Leak Detection by Acoustic Signal Analysis
Applied Acoustic, 33 (1991) 1-19

[3] IAEA-Report
The Safety of Nuclear Power Plants in Central and Eastern Europe
IAEA-Rosen.cha / 91, (1991) p. 13

[4] Gesellschaft für Reaktorsicherheit (GRS) GmbH
Sicherheitsbeurteilungen des Kernkraftwerkes Greifswald, Block 5 (WWER-440/W-213)
GRS-83 (August 1991), S. 58

[5] Kretschmar, W.
Programmbeschreibung MICRO FUCS - Fuzzy Classification System
Institut für Mechanik, Chemnitz, 1991

[6] Loos, M.
Bedienhandbuch NEUROPRO
MEDAV Schrift Nr. 394, Uttenreuth, 1992.

[7] Rumelhart, D., G. Hinton, R. Williams
Learning representations by backpropagating errors
Nature, 323 (1986) 533 - 536

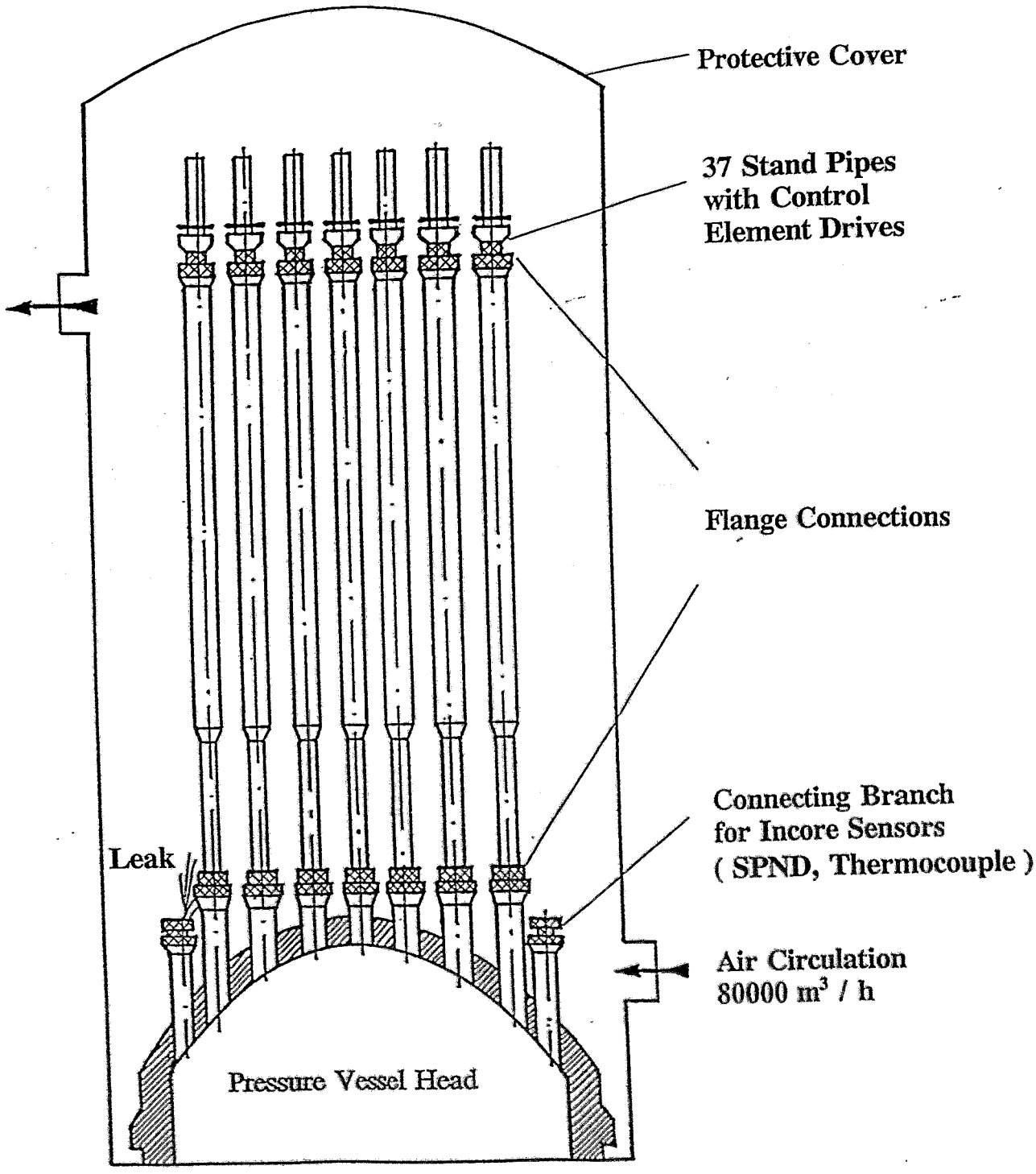

Fig.1 Scheme of the pressure vessel head (upper block of VVER-440)

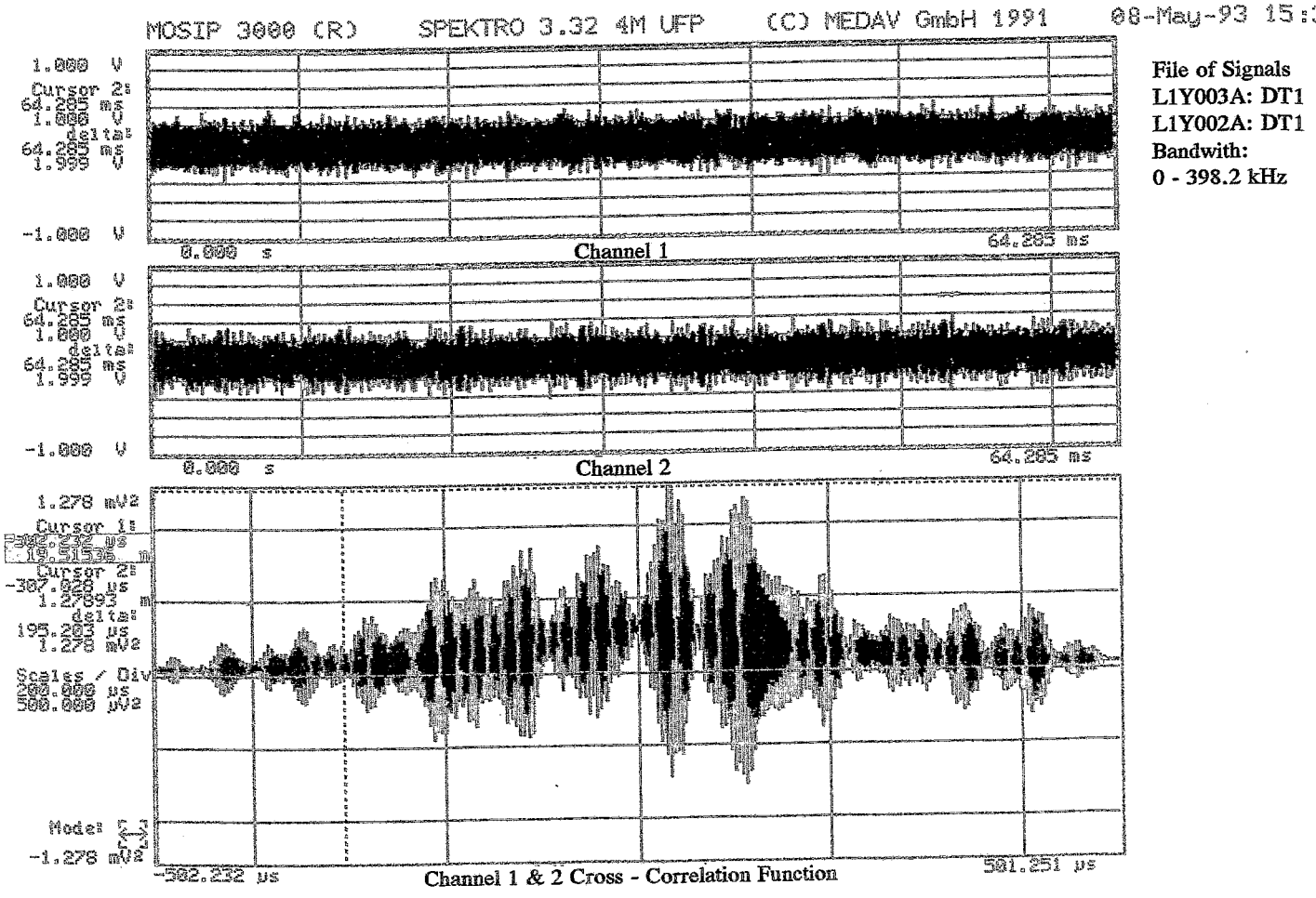

Fig.2 AE-sensor signals and cross-correlation function
leak position: SUS 06-31, channel 1: AE3 (SUS 18-55)
channel 2: AE2 (SUS 03-46)

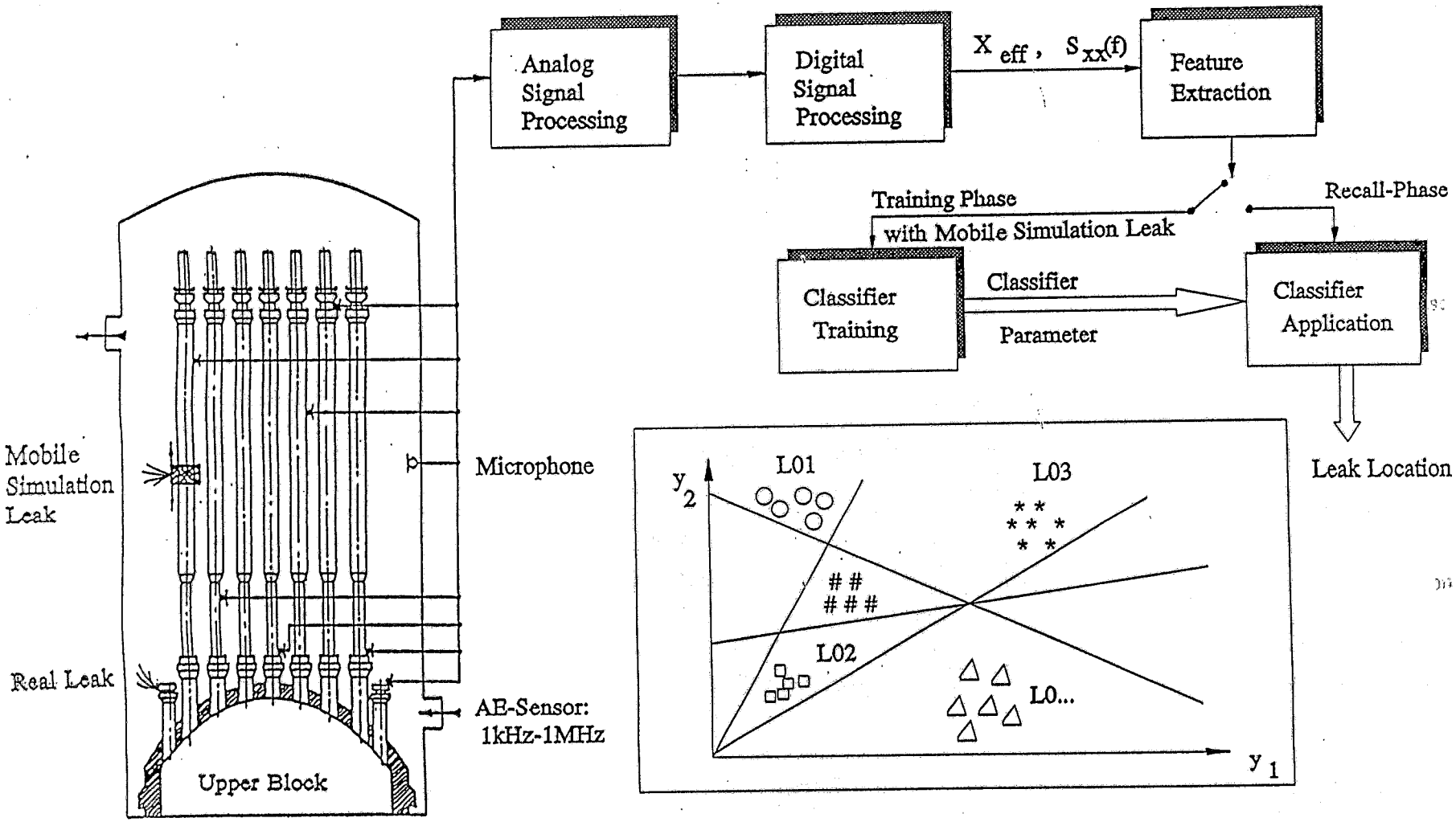

Fig.3. Leak location at complicated structures.

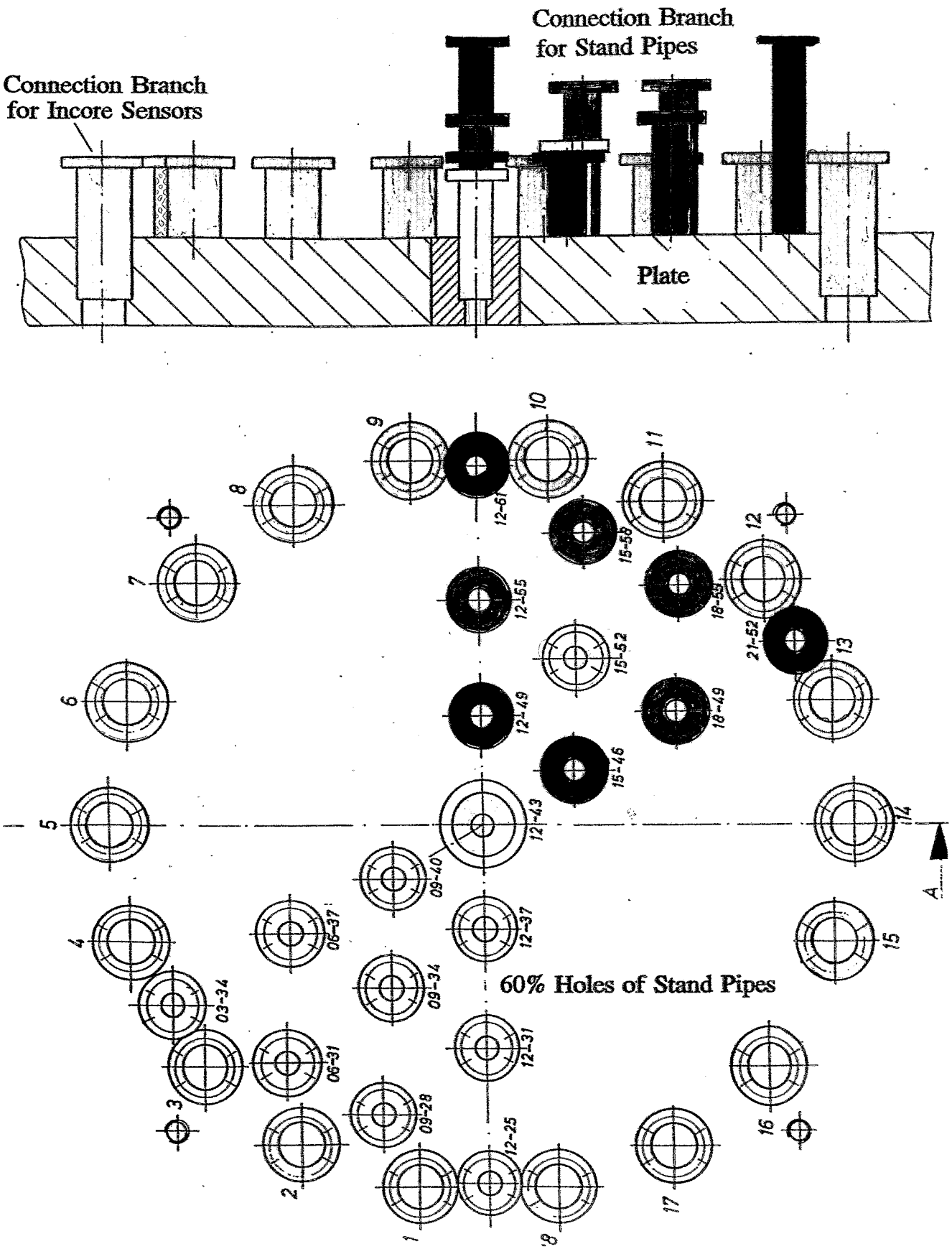

Fig.4. Scheme of acoustic 1:3 model of the upper block

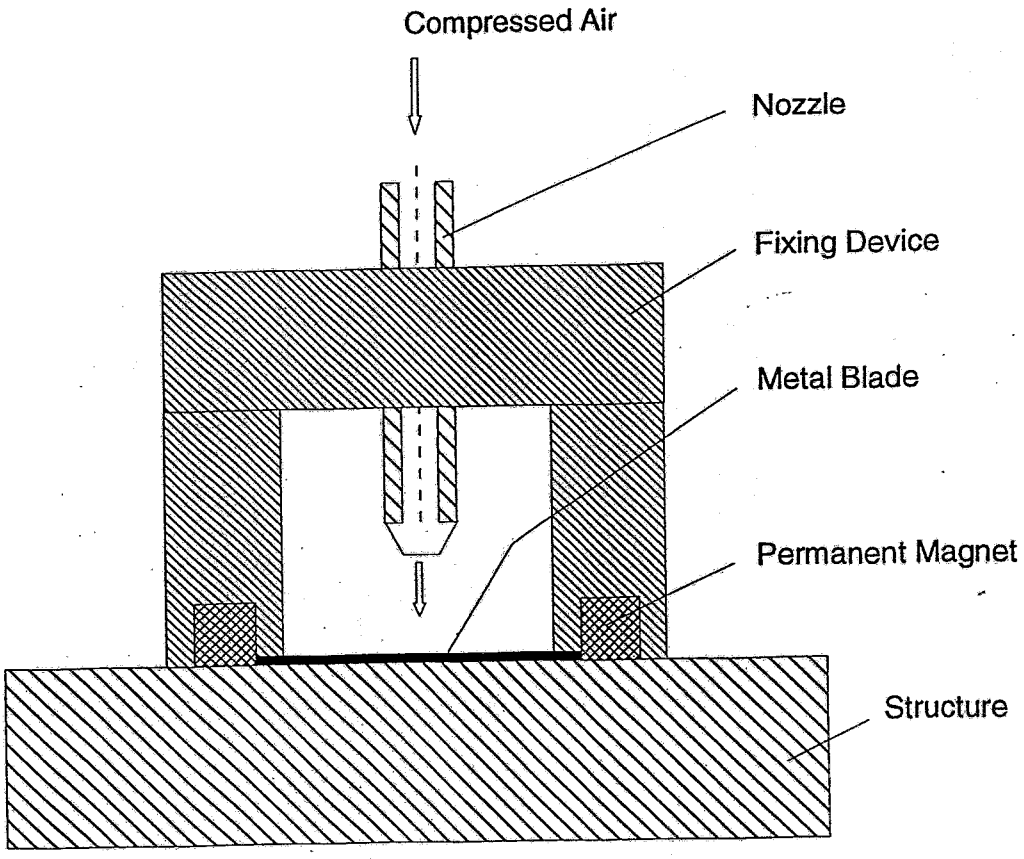

Fig. 5 High-frequency sound source consisting of a thin metal blade coupled to the structure with silicon oil and excited through a jet of compressed air.

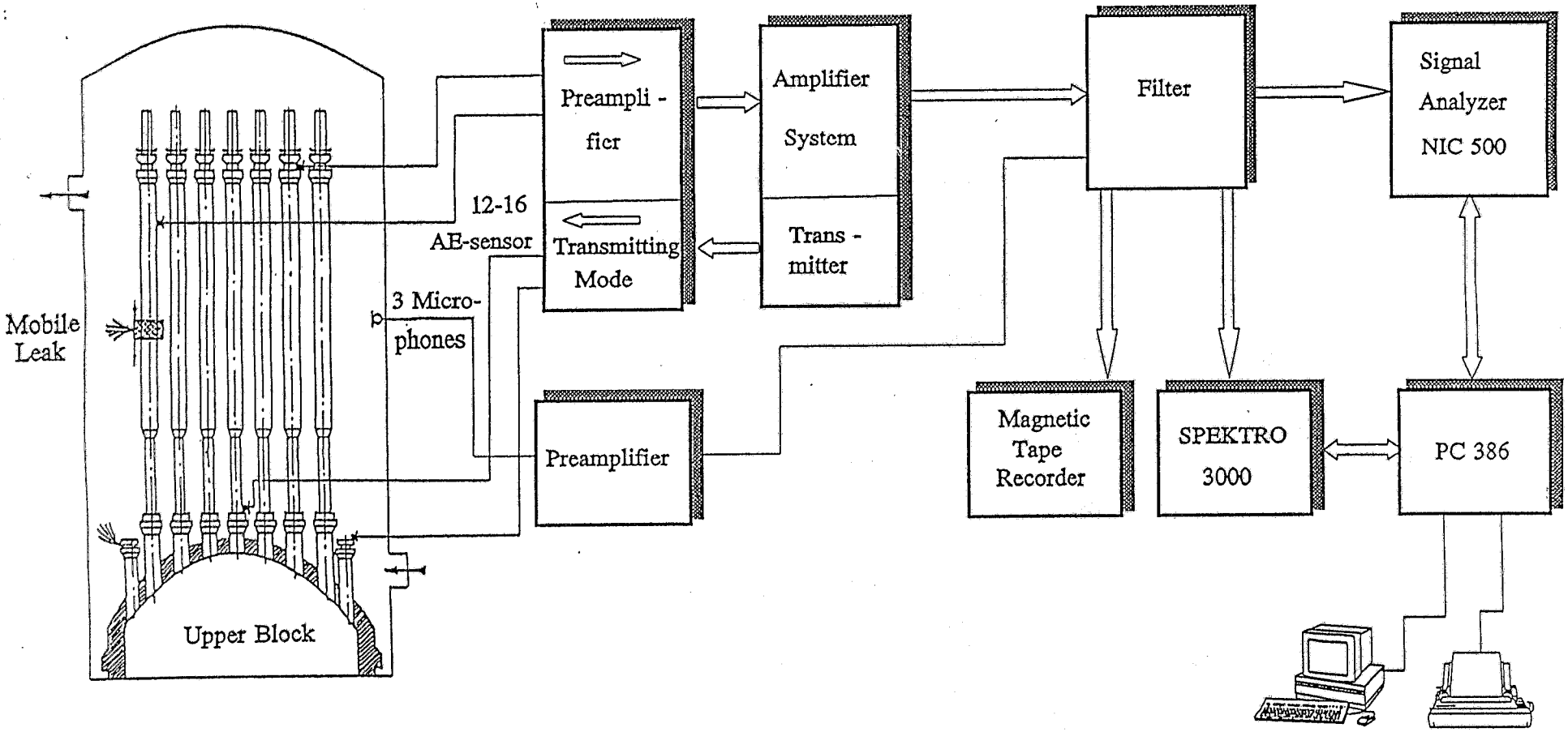

Fig. 6 Measuring equipment and signal processing system for leak simulation experiments

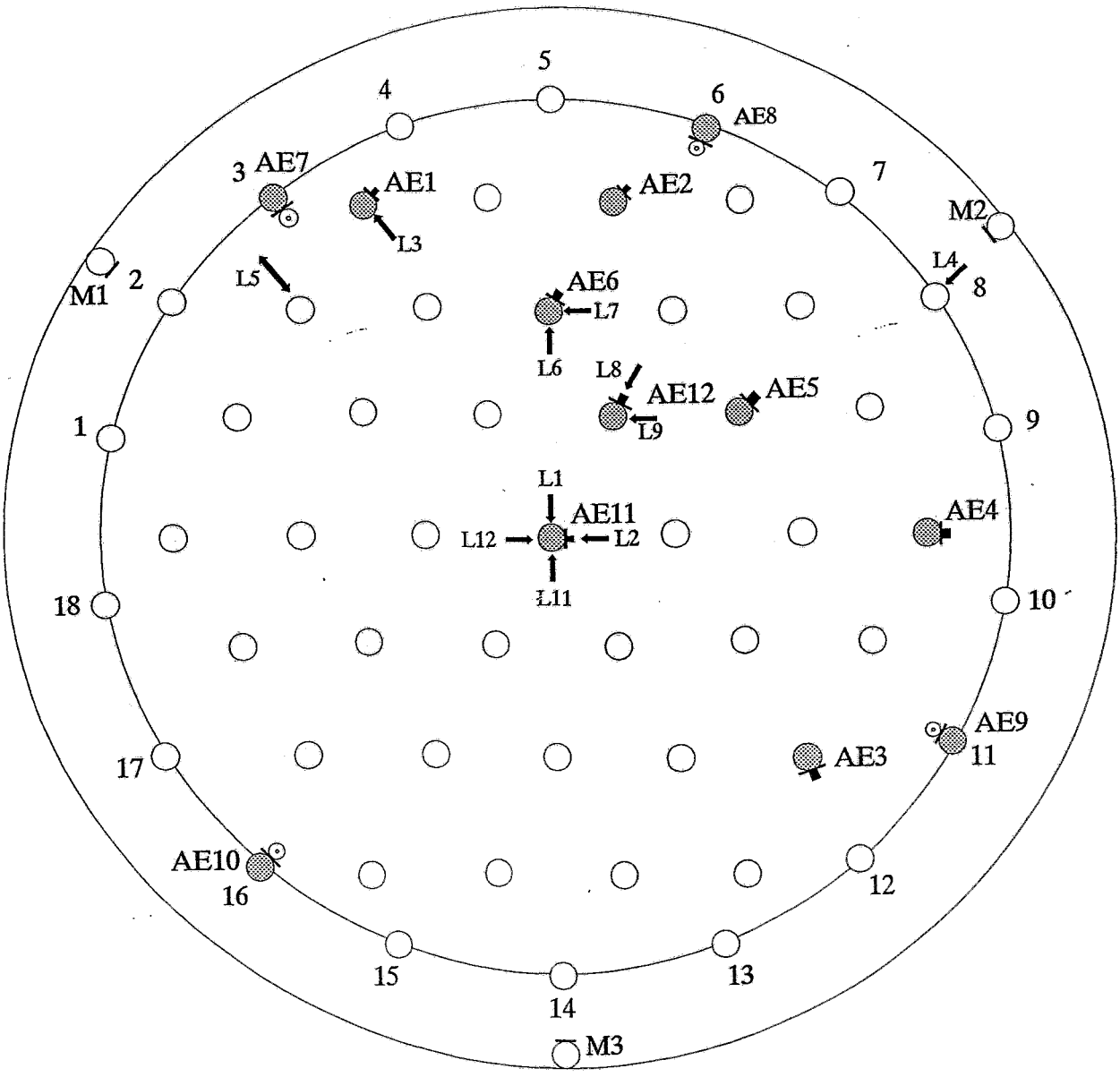

Fig. 7: Positions of microphones (MICn), AE-sensors (AEn) and leaks (Lm) simulated by a compressed air jet, at the pressure vessel head

- microphone at the wall of the protection vessel
- AE-sensor at the lower flange of the standpipe
- AE-sensor at the connecting branch for incore sensors
- jet direction
- leak at the top of the standpipe

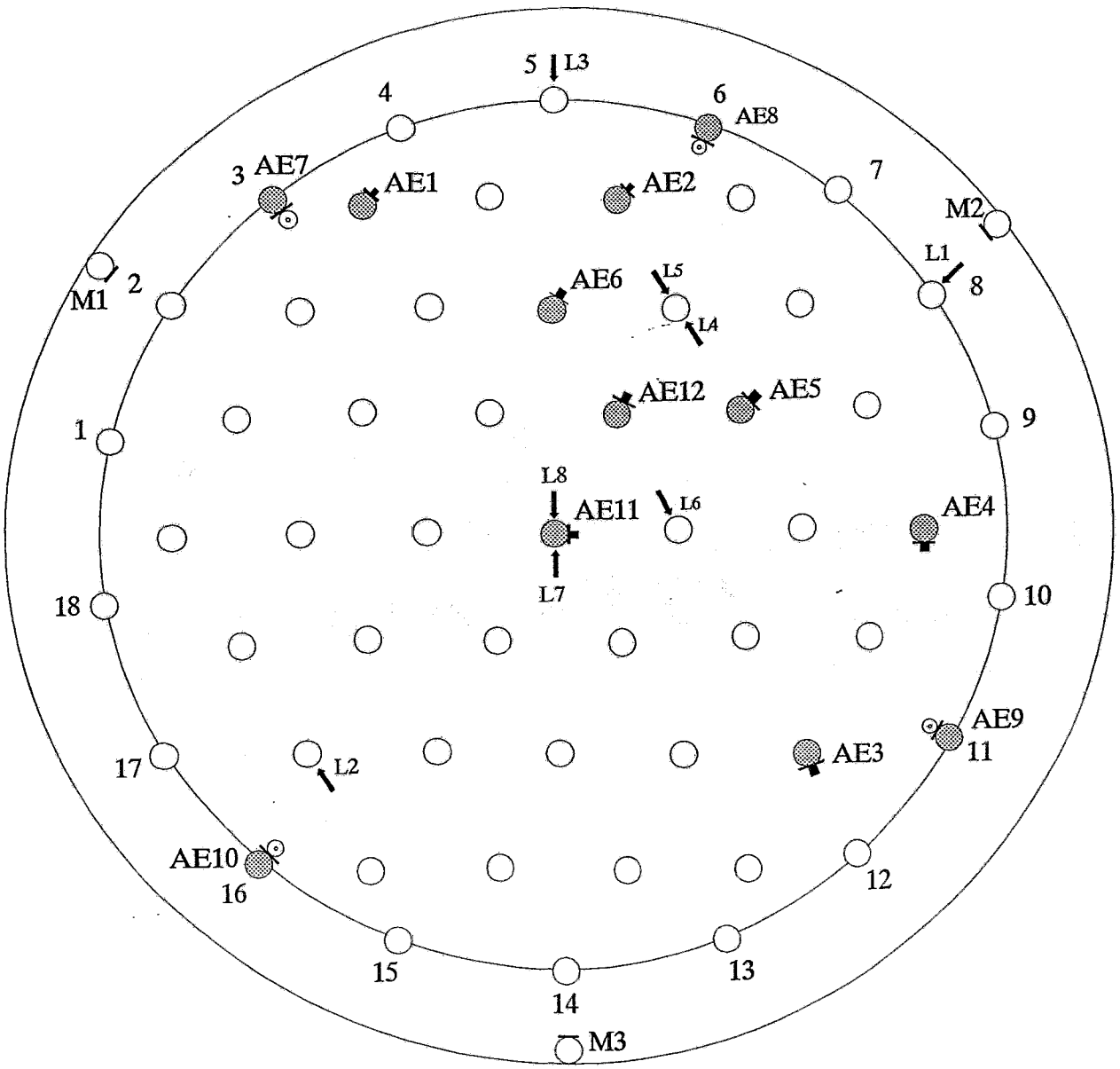

Fig. 8: Positions of AE-sensors (AEn) microphones (MICn) and leaks (Lm) simulated by a high-frequency sound source at the pressure vessel head

- AE-sensor at the lower flange of the standpipe
- AE-sensor at the connecting branch for incore sensors
- microphone at the wall of the protection vessel
- jet direction

Classifier A

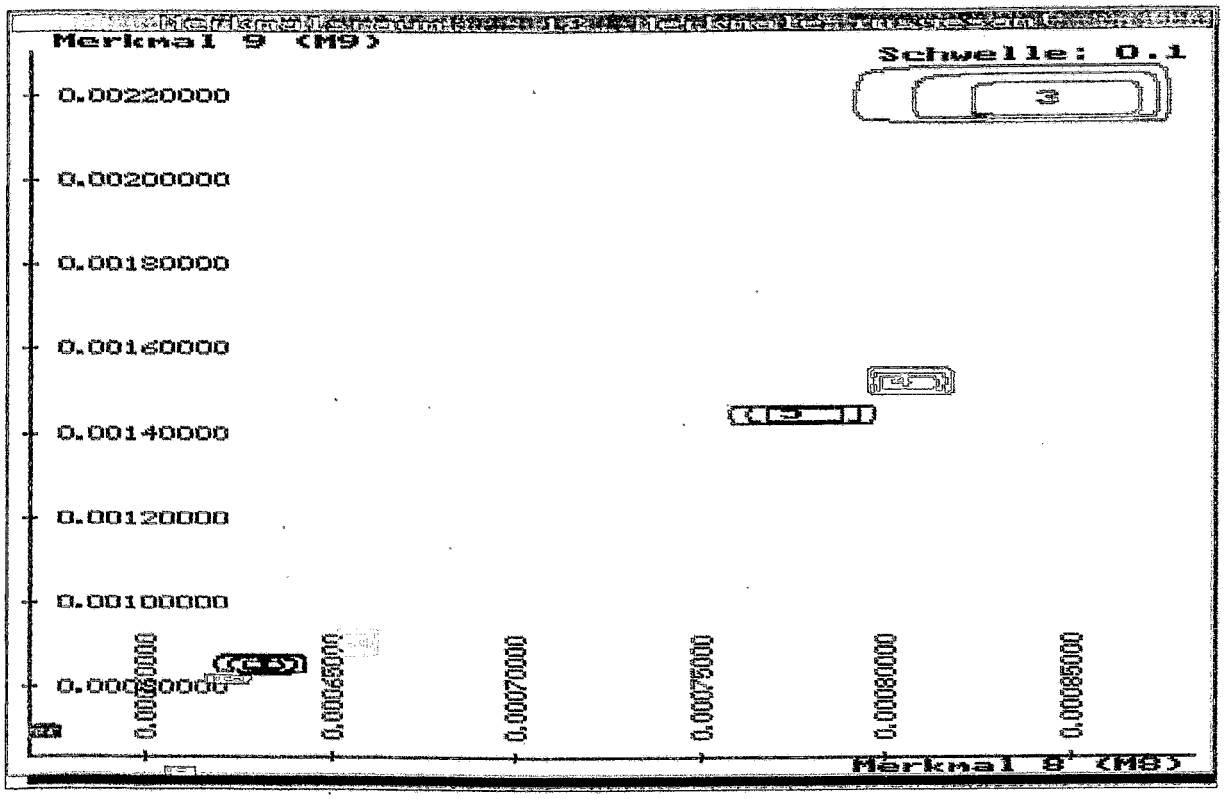

Classifier B

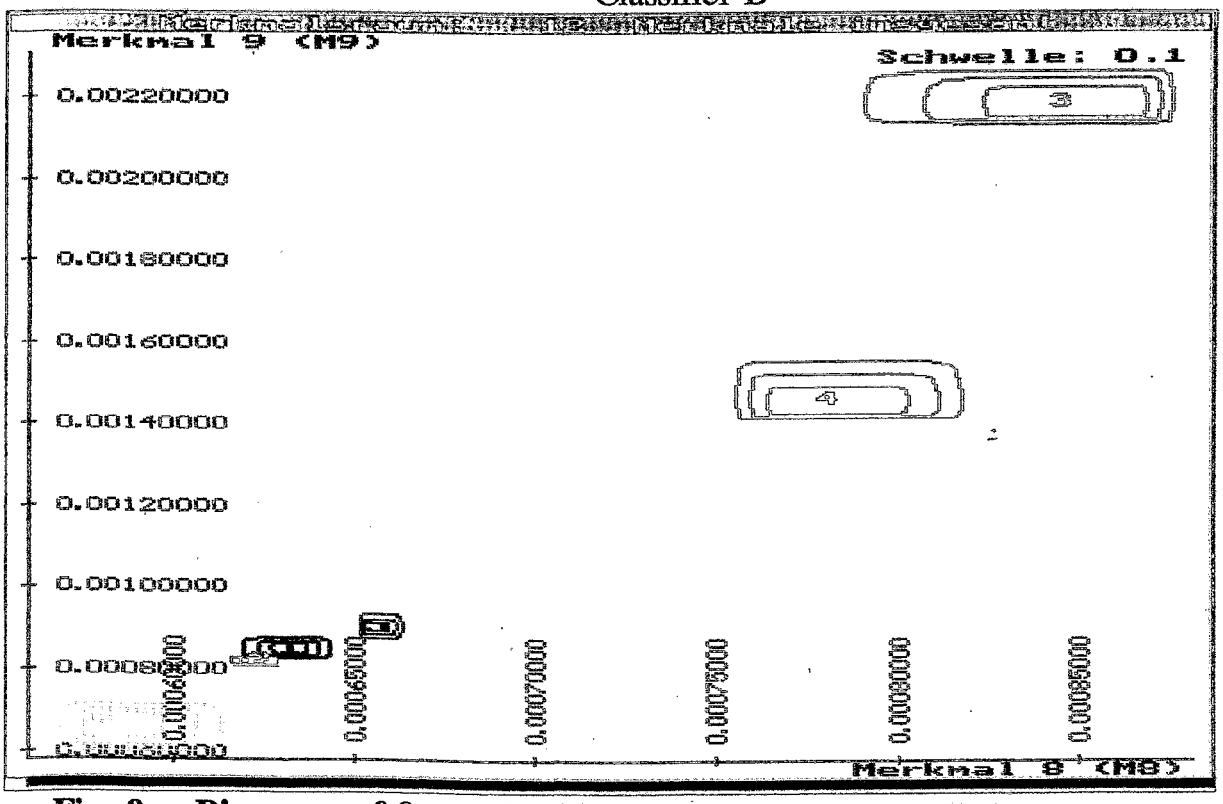

Fig. 9 Diagrams of fuzzy classifiers for rms-values of AE-signals

Classifier A separate classes for each simulated leak (8 classes)
Classifier B joined classes for leaks at the same standpipe flange (classes 4 and 5)

Classifier A

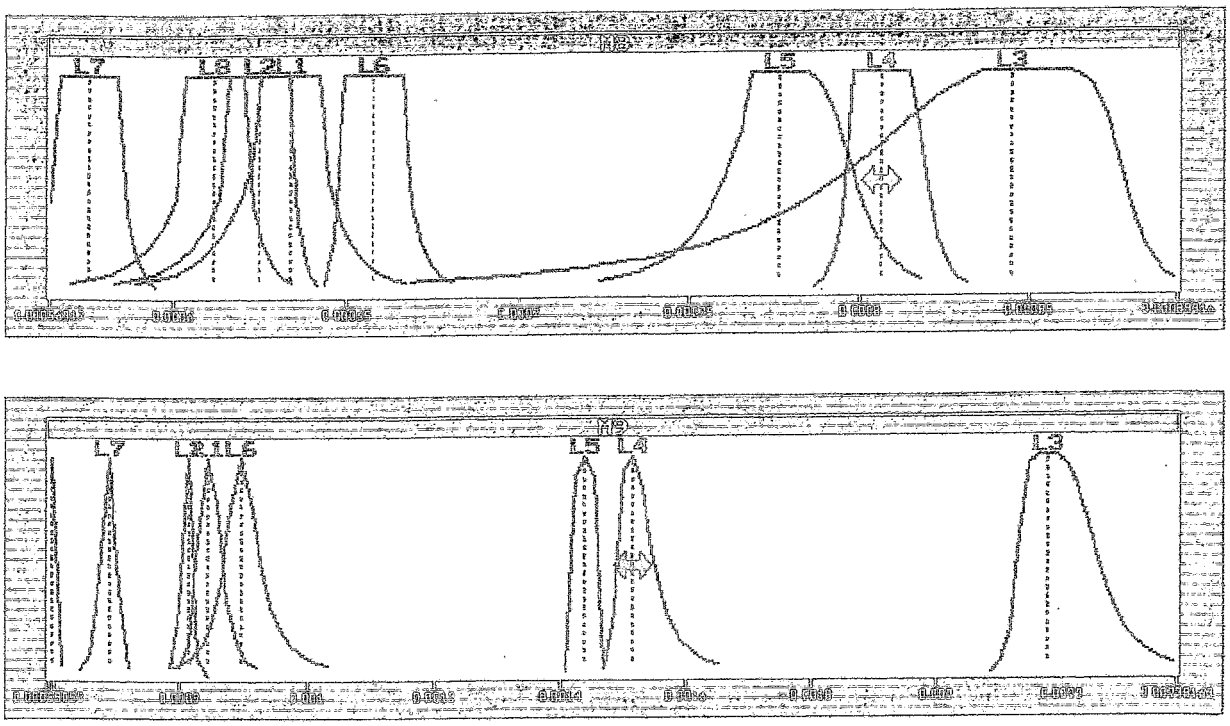

Classifier B

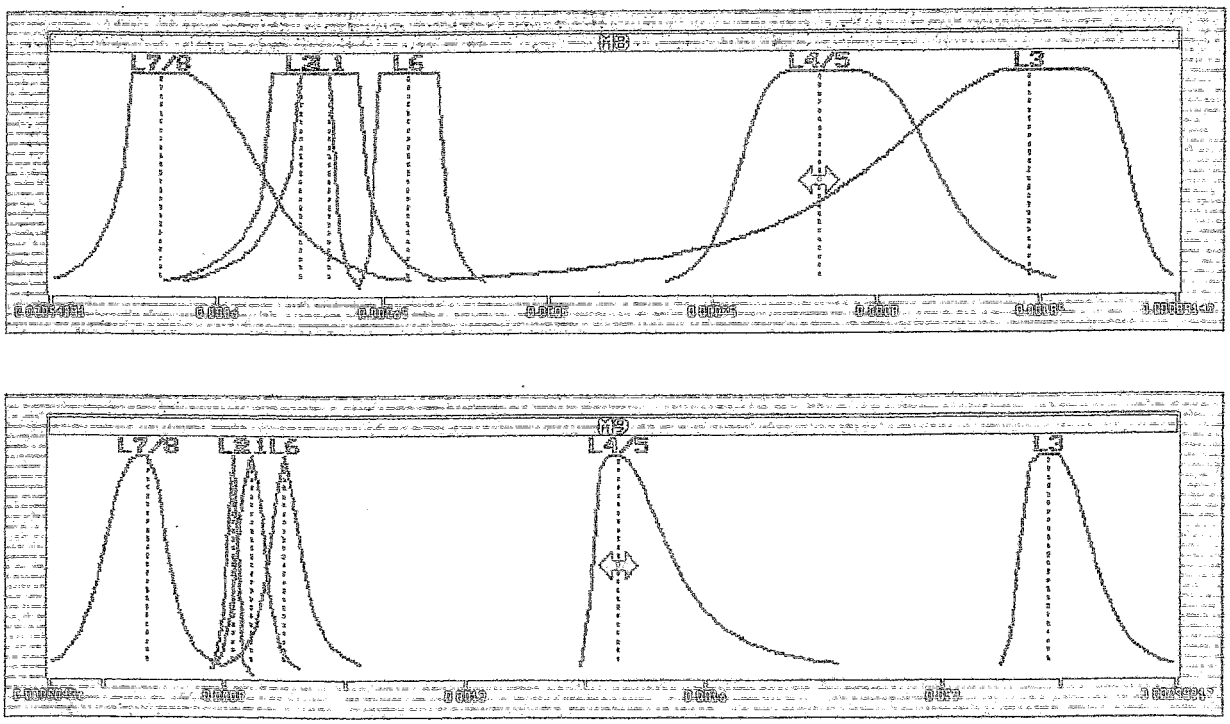

Fig. 10 Membership functions of the features M8 (AE8) and M9 (AE9) for the two Fuzzy classifiers A and B

L4, L5 separate membership functions trained with opposite leak positions at the same standpipe flange

L4/5 joint membership functions trained with opposite leak positions at the same standpipe flange

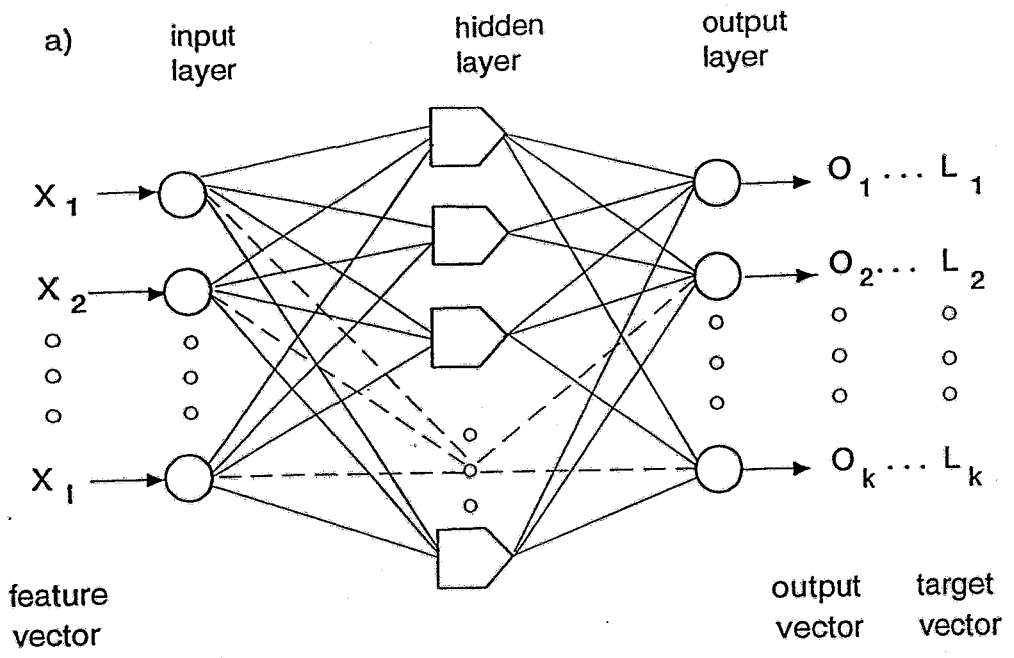

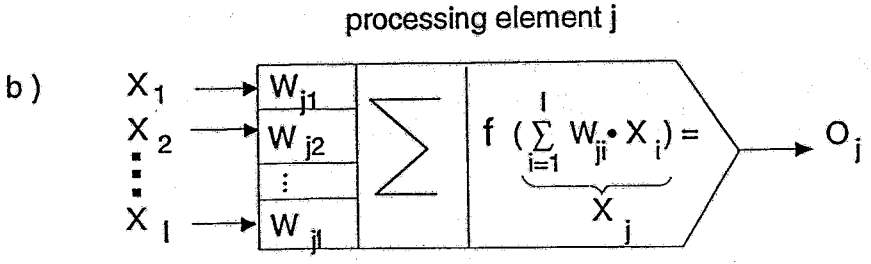

sigmoid function $f = 2 / (1 + e^{-2x}) - 1$

c)

error $\delta_j = f'(\sum_i W_{ji} \cdot X_i) \cdot \sum_j W_{kj} \cdot \underbrace{f'(\sum_j W_{kj} \cdot X_j) \cdot (L_k - O_k)}_{= \delta_k}$

weight $W^*_{ji} = W_{ji} + \alpha \delta_j \cdot X_i$

α learning rate

Fig.11 Multilayer perceptron network

a) Structure of the neutral network

b) Processing element j of the hidden layer

c) Error backpropagation rule

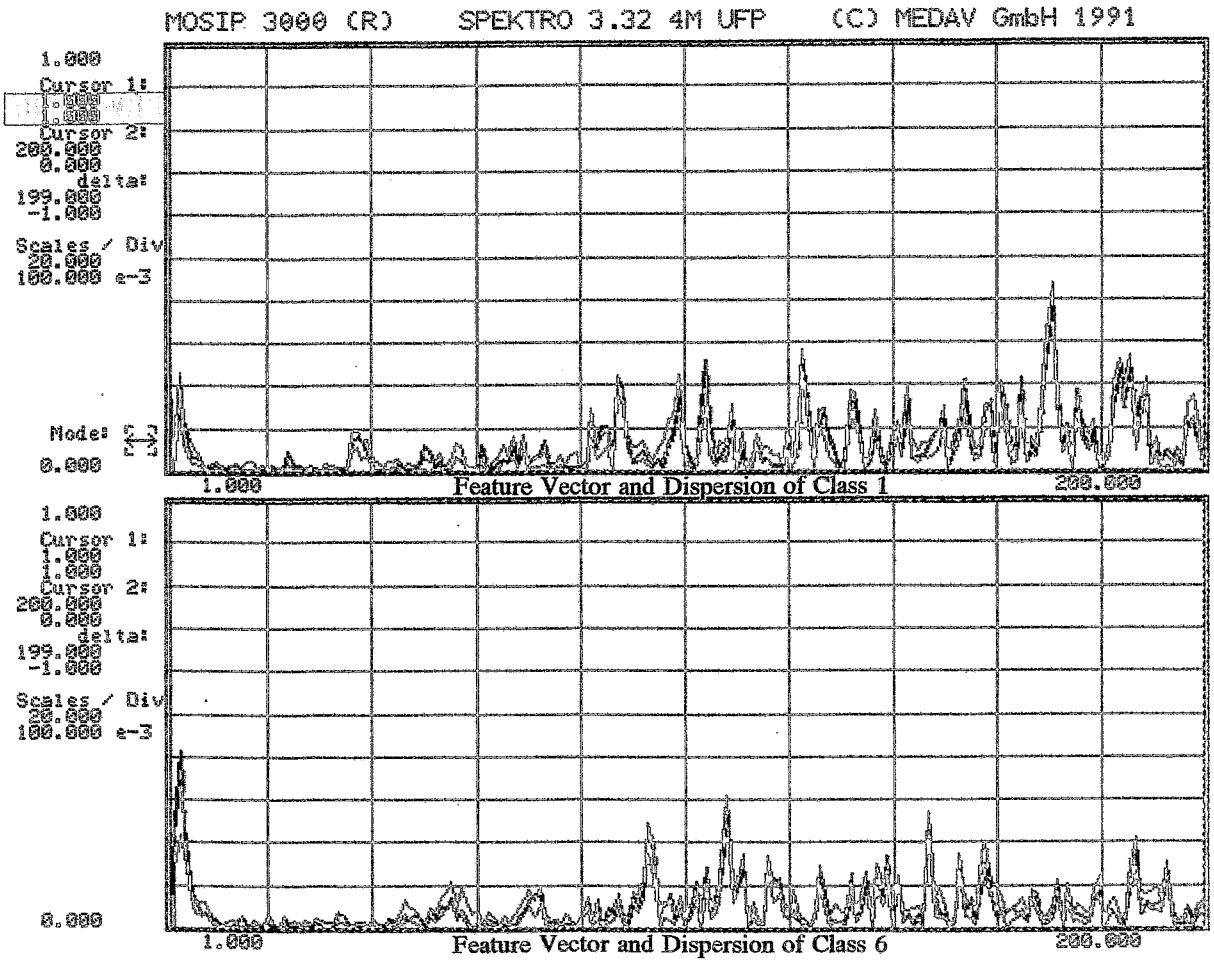

Fig. 12 Feature vectors and dispersions of class 1 and class 6

dark blue	selected feature vector
light blue	range of dispersion

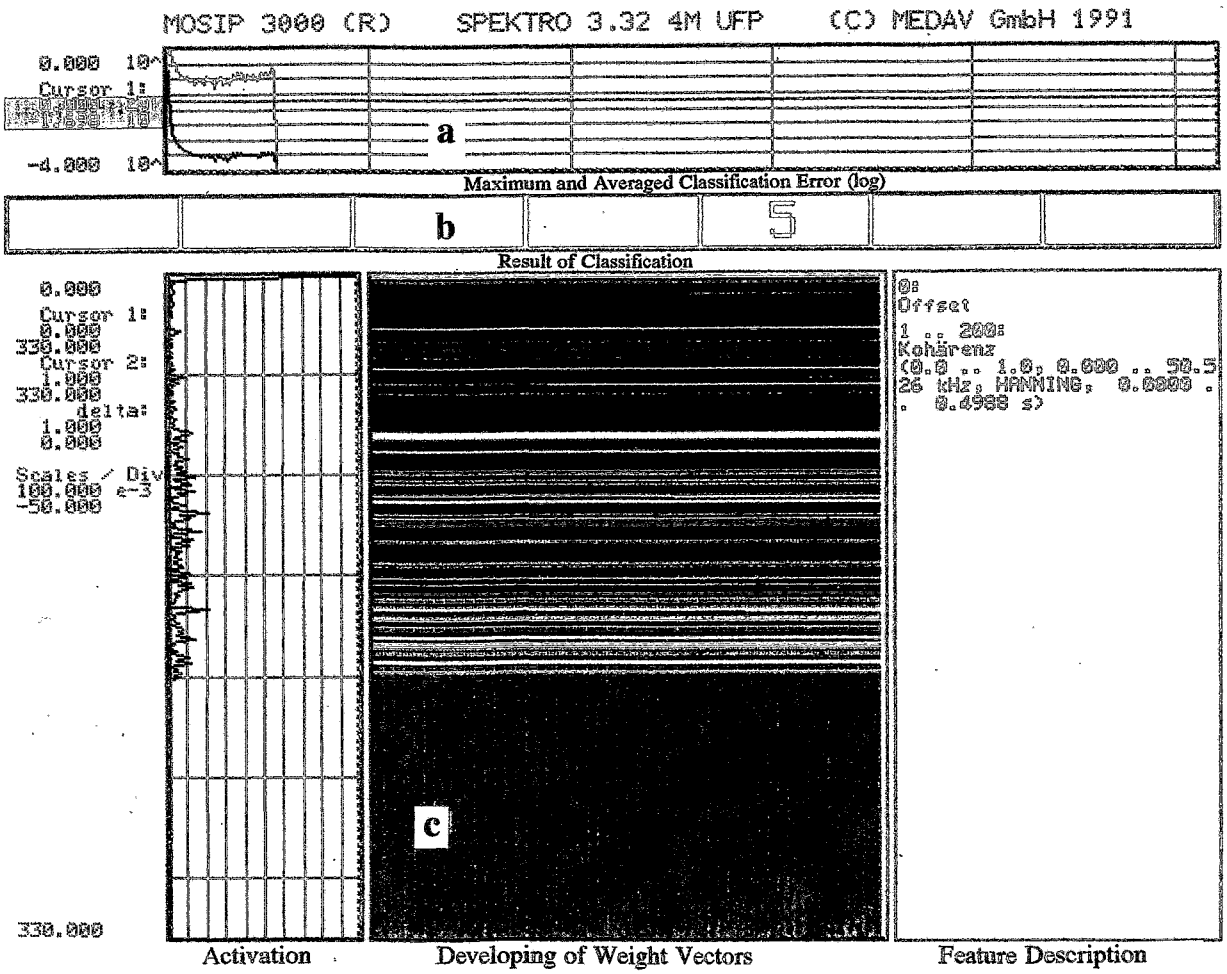

Fig. 13 Training of a two-tayer perceptron network P1 (without hidden layer)

a) Maximum and averaged classification error (log)
b) Number of the recognized class
c) Connection strengths between the 200 input neurons and output neuron number 5
red = high weight, blue = low weight

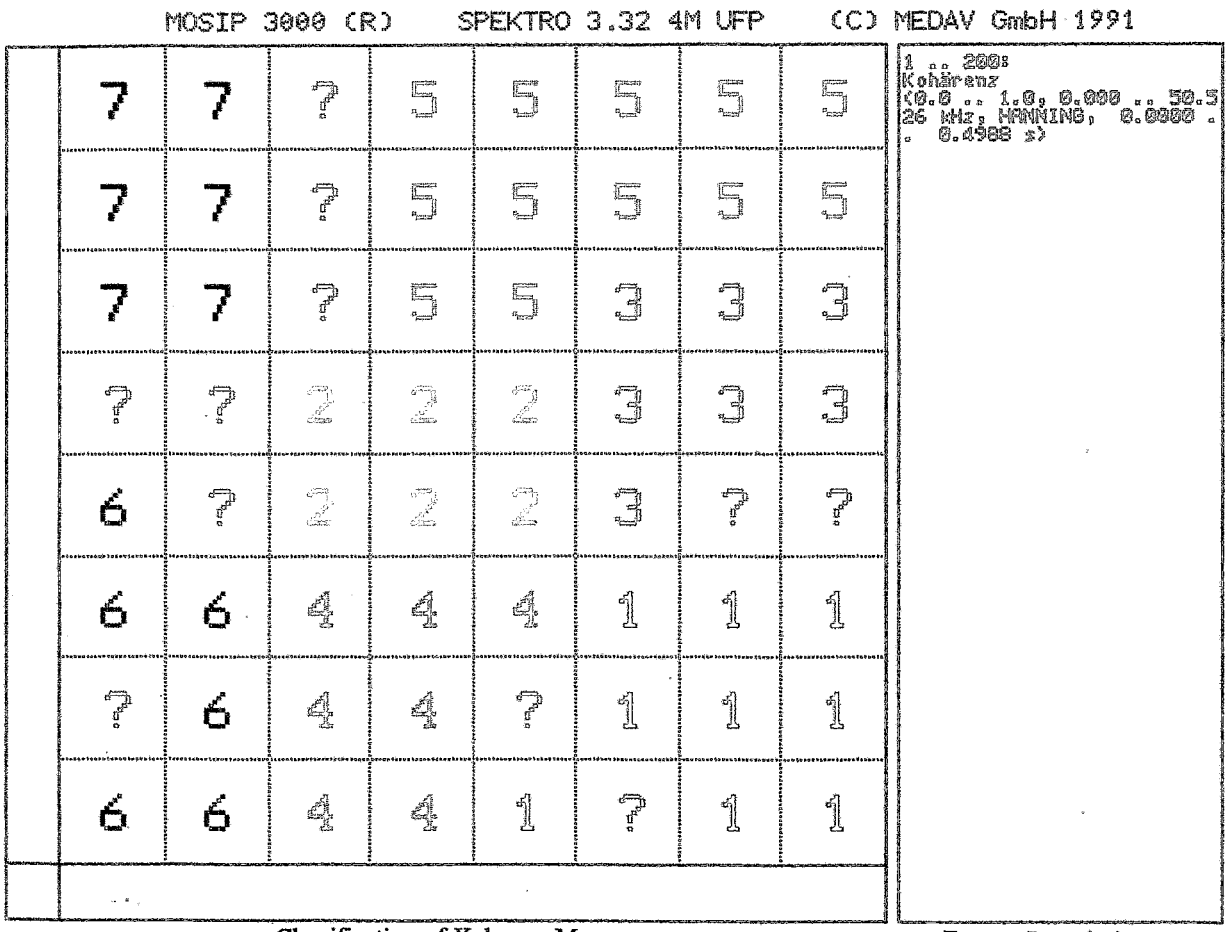

Fig. 14 Kohonen-map of the counterpropagation network CPP

?) = Cancelled neurons related to various classes

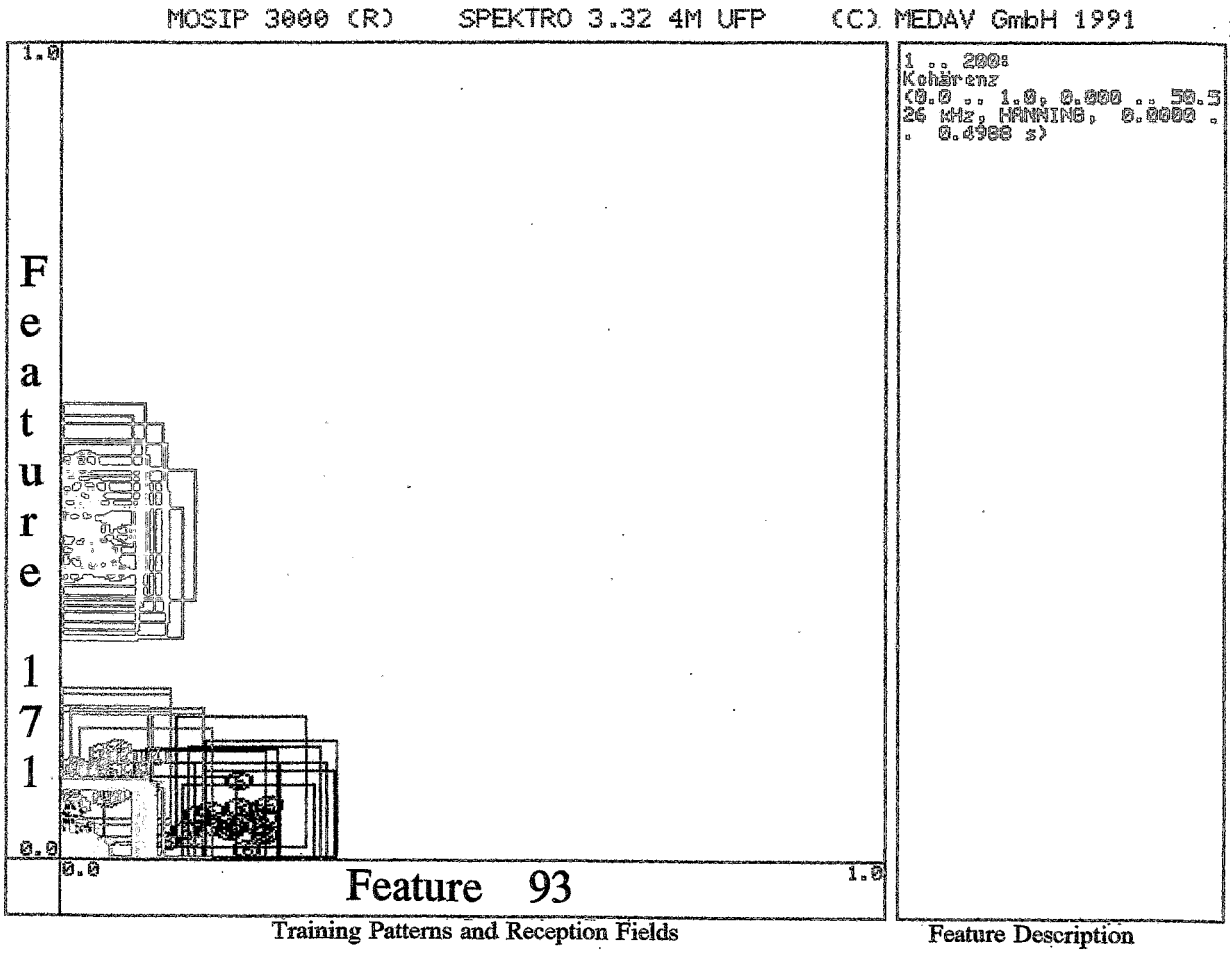

Fig. 15 **Diagram of training patterns and reception fields for hidden-layer neurons of the condensed-nearest-neighbour network CNN and for features 171 and 93**

⑥ training pattern of class 6 □ reception field of a neuro

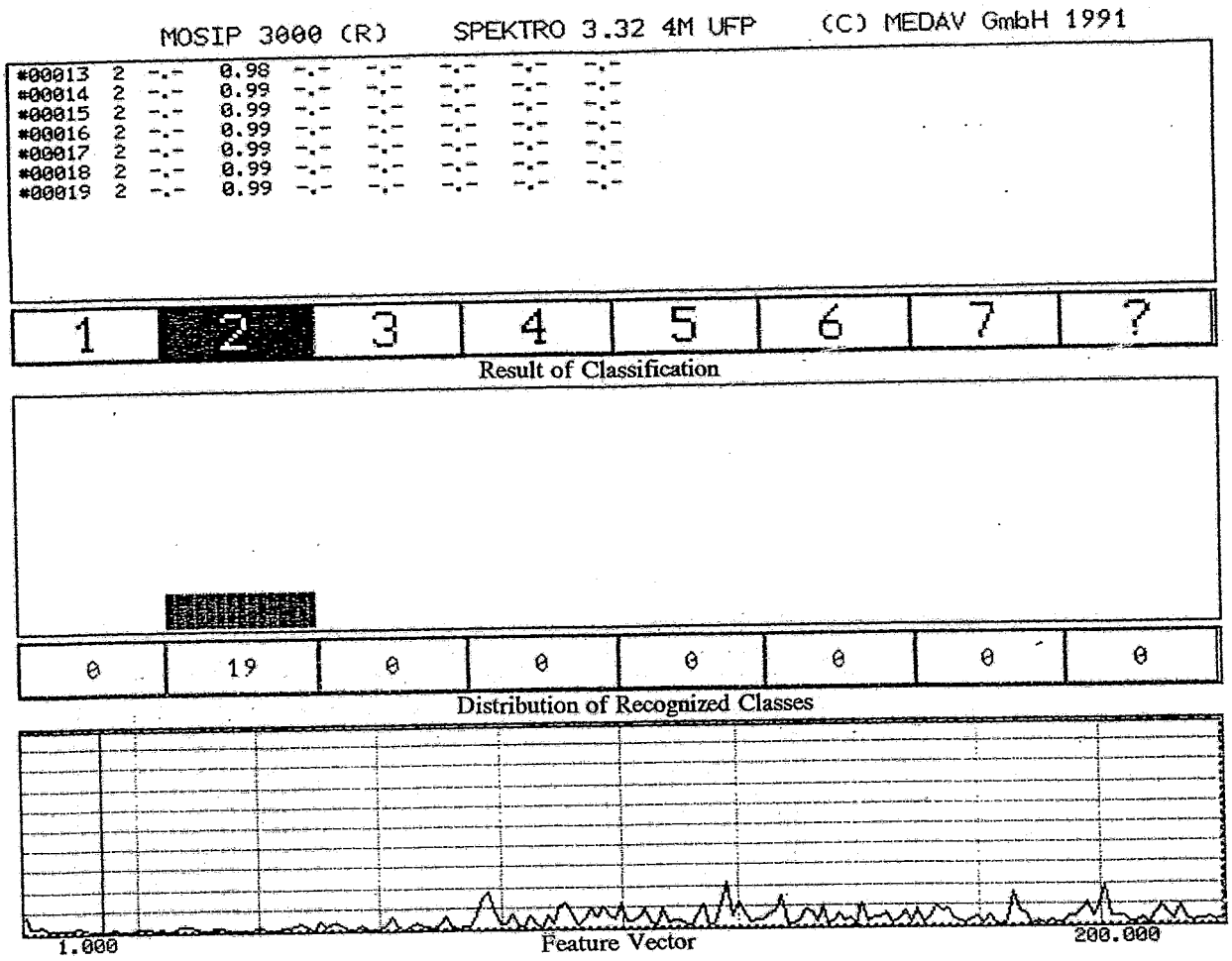

Fig. 16 **Classification by means of a two-layer perceptron network P1 with sigmoid activation function and coherence function as feature vector**

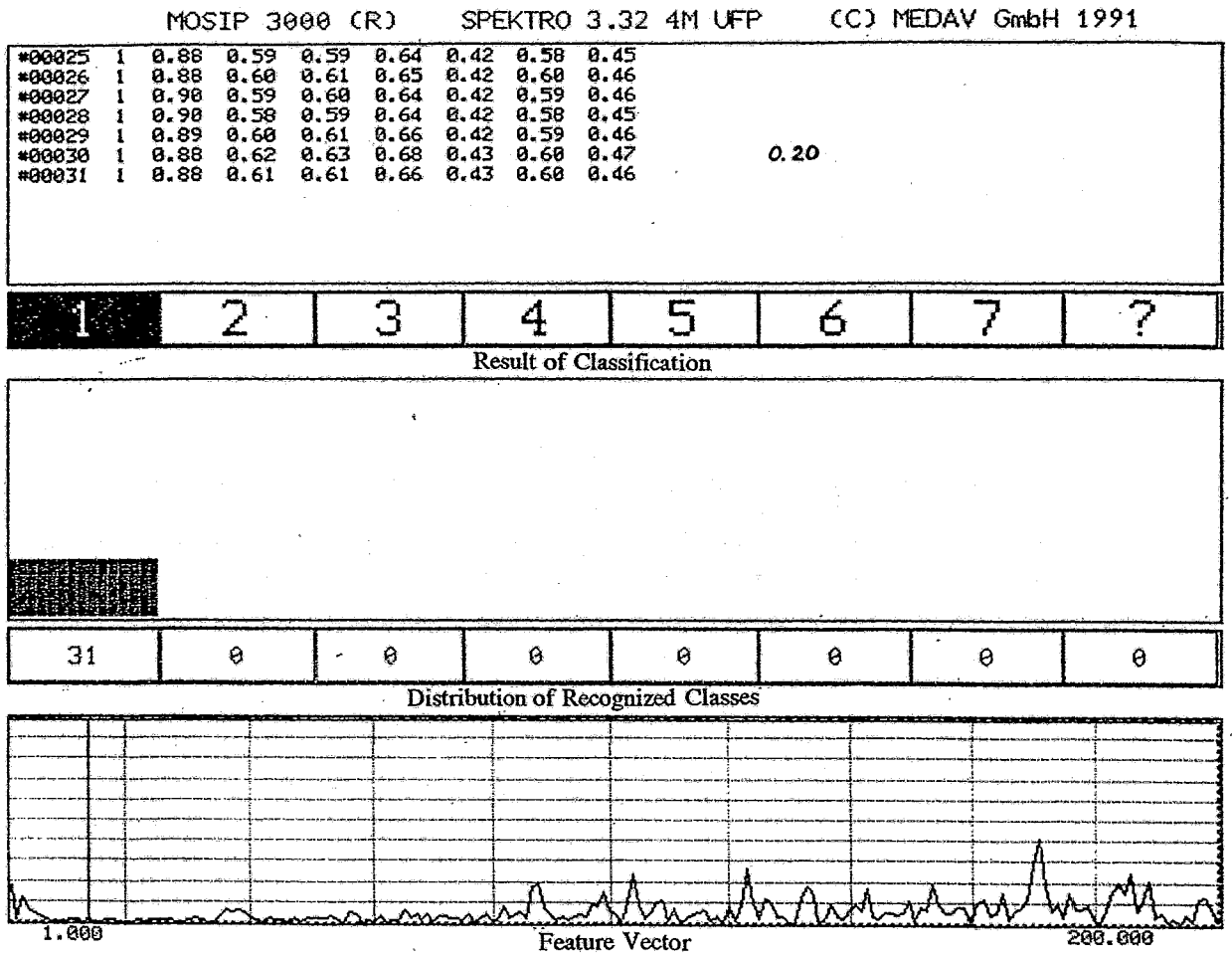

Fig. 17 **Classification by means of a counterpropagation network CPP with coherence function as feature vector**

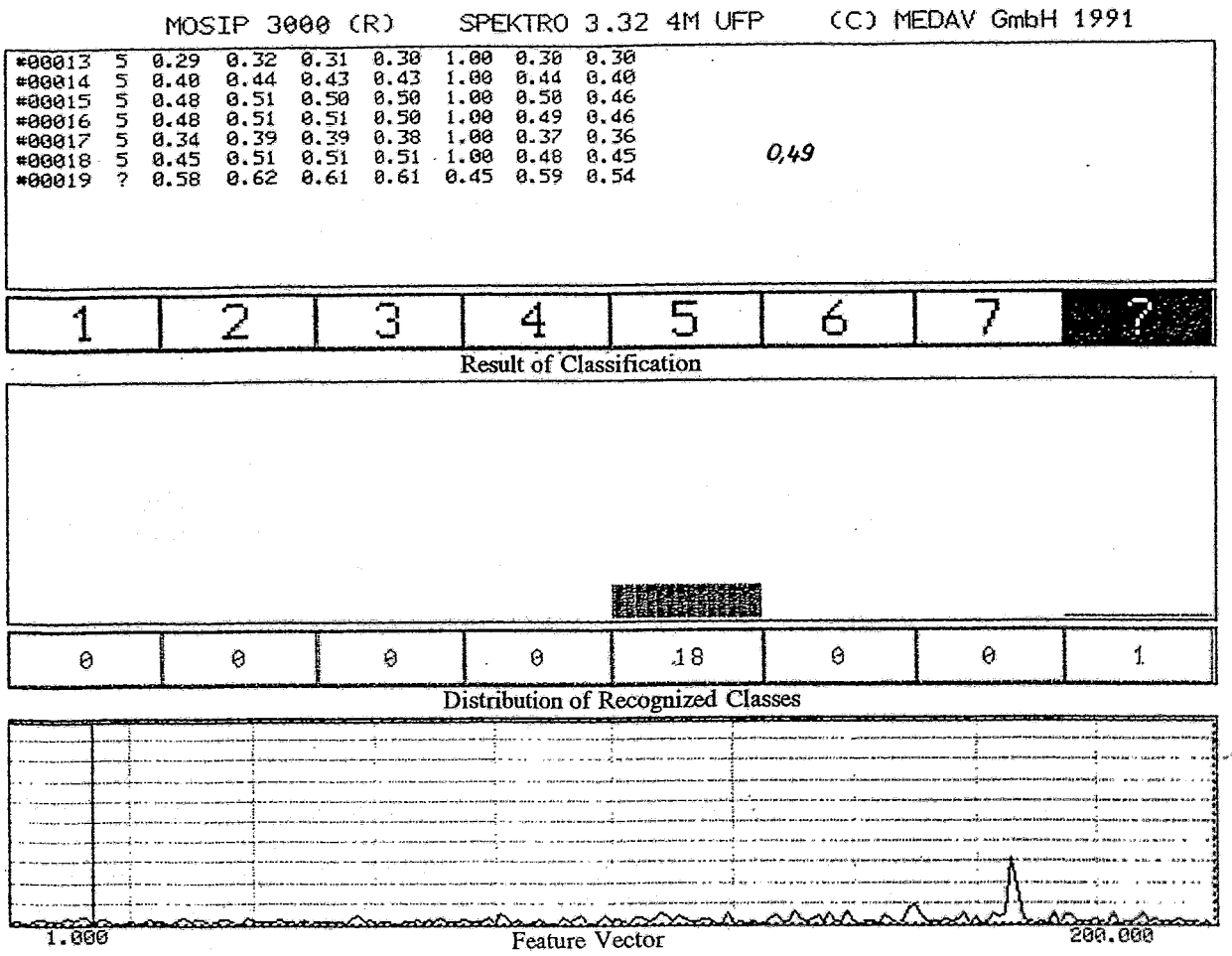

Fig. 18 Classification by means of a condensed-nearest-neighbour network CNN with coherence function as feature vector

?) = rejection class

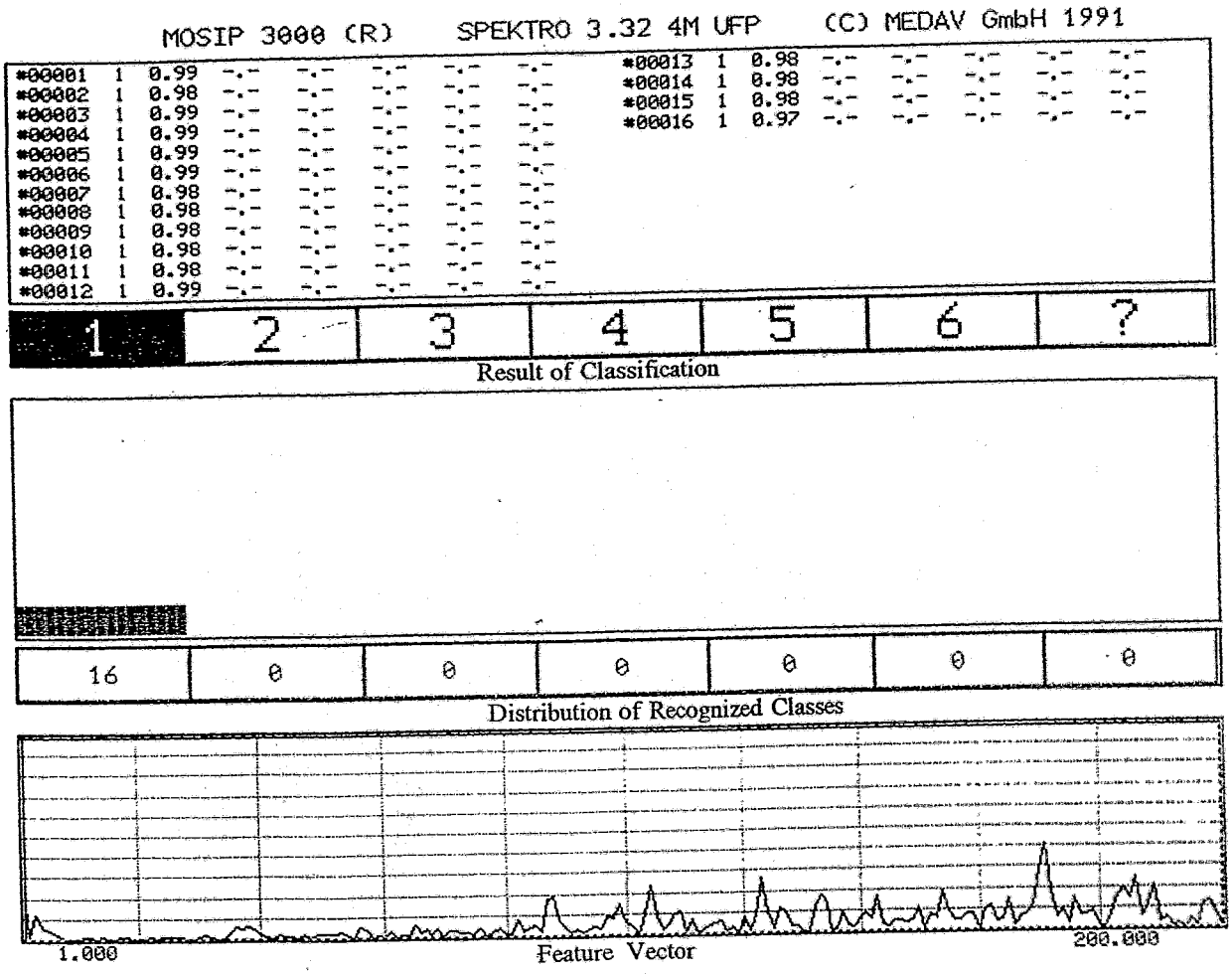

Fig. 19 **Classification by means of a three-layer perceptron network P2 with error backpropagation, sigmoid activation function and coherence function as feature vector**